Analysis of the Coupling of Overhead Lines Excited by Indirect Lightning Considering Dispersive Soil Water Percentage

Analysis of the Coupling of Overhead Lines Excited by Indirect Lightning Considering Dispersive Soil Water Percentage

Chengpan Yang, Feng Zhu, Riccardo Trinchero, *Member*, *IEEE*, and Igor Simone Stievano, *Senior Member*, *IEEE*

***Abstract*—This paper proposes a method to analyze the coupling of overhead lines excited by indirect lightning above the dispersive soil, considering the change of soil water percentage. The whole process is achieved through analytical equations. Firstly, the two-dimensional finite-difference time-domain method with convolution perfectly matched layer boundary based on the Debye representation of frequency-dependent ground is used to calculate the lightning electromagnetic field. In the frequency domain, the vector fitting method is introduced to deal with the frequency-dependent part of the governing equations. The recursive convolution is then combined with the integration by parts to process the convolution part of the governing equations of overhead lines in the time domain, enhancing the robustness of the solution. The resulting iterative equation is in turn derived, allowing to solve the problem at hand, for line loads defined by either *R-C* parallel or *R-L* series loads. The results highlight that, with respect to purely resistive loads, inductive loads increase the coupling voltage and reduce the coupling current, while capacitive loads do the opposite. In addition, the coupling value is verified to be more sensitive to changes in water percentage at low soil water quantity.**

***Index Terms*—overhead lines, lightning, finite-difference time-domain (FDTD), vector fitting (VF), Longmire and Smith (LS) model.**

I. INTRODUCTION

DIRECT lightning is a visible hazard to the power system, which has a very strict protection system [1]. However, the damage caused by indirect lightning to electrical systems is difficult to detect, as indirect lightning may induce voltage or current on surrounding conductive objects. The indirect lightning has abundant harmonic energy in the frequency band whose wavelength is comparable to the length of the overhead lines, which are usually on the order of kilometers [2]. Lightning and overhead lines have a large coupling area, the induced voltage or current can pose potential risks to terminal loads. Therefore, accurate calculation and evaluation of the coupling effect of indirect lightning and overhead lines have positive effects on power system protection.

The change of soil electrical parameters (conductivity σ_g and dielectric constant ε_g) will directly affect the propagation of lightning electromagnetic field [3], and at the same time affect the ground impedance of the overhead lines model [4]. In addition, the variation of soil electrical parameters with frequency, also known as the dispersion characteristics of soil [5], [6], is influenced by soil water percentage [7]-[9]. Therefore, the influence of dispersive soil on the lightning electromagnetic field (EMF) coupling to the transmission line model cannot be ignored.

The method for solving the coupling value of overhead lines excited by indirect lightning can be divided into solving the lightning EMF and the governing equations of the filed-to-wire coupling model [10]. Delfino analyzed the influence of soil with different water percentages on the lightning EMFs through the soil model proposed by Longmire and Smith (LS) [3]. And the EMFs of the first return stroke (FRS) and subsequent return stroke (SRS) on the ground and underground were analyzed by different calculation methods, however, both solve complex Sommerfeld integrals [11], which converges slowly, especially when dealing with long transmission lines problem. The commercial software COMSOL based on the finite element method (FEM) [12] has also been used to solve the lightning EMF in the case of dispersive soil [8][13], which needs to be combined with the inverse Fourier transform to achieve the solution of the time-domain lightning EMF. Under the balance of accuracy and running time, approximate solutions can only be obtained at some frequency points, which inevitably increases errors. However, the finite-difference time-domain (FDTD) method [14] can directly calculate the time domain results without solving the tedious inverse Fourier transform. If the lightning environment is open or symmetrical, the three-dimensional lightning EMF can be solved using more efficient two-dimensional (2D) model. Yang was the first to apply 2D-FDTD with Mur (Gerrit Mur) boundary condition to solve the lightning EMF [15]. In order to improve the absorption efficiency of the boundary and achieve faster solution speed, the convolution perfectly matched layer (CPML) boundary [16]

Corresponding author: Feng Zhu.
C. Yang and F. Zhu are with the National Rail Transit Electrification and Automation Engineering Technique Research Center, and the School of Electrical Engineering, Southwest Jiaotong University, Chengdu 611756, China (e-mail: ycp@my.swjtu.edu.cn; zhufeng@swjtu.cn;).
R. Trinchero and Igor S. Stievano are with the EMC Group, Department of Electronics and Telecommunications, Politecnico di Torino, Turin 10129, Italy (e-mail: riccardo.trinchero@polito.it; igor.stievano@polito.it;)

is introduced to solve the lightning EMF [17], [18], which is independent of the medium and can be efficiently applied to dispersive media [19], [20]. For dispersive soil, Sun proposed a 2D-FDTD method for lightning EMF using semi analytical recursive convolution [5]. On the basis of [5], Kurnaz combined with the Debye representation of frequency-dependent ground to propose a more excellent 2D-FDTD method [20].

The commercial software COMSOL based on the FEM and perfectly matched layer (PML) boundary conditions is also used to solve the coupling voltage of the overhead lines excited by lightning in the case of dispersive soil [8] [13], but it cannot provide analytical equations. Meanwhile, the CPML boundary has more advantages than the PML boundary, such as being very effective in attenuating evanescent waves and reducing reflections [16]. Based on the Alipio and Visacro (AV) soil model, the coupling voltage of overhead lines above the dispersive soil ground excited by lightning EMF was solved in [6], but the influence of underground electric fields was not considered. Compared with the AV soil model, the LS soil model can more directly reflect the impact of soil water percentage changes on soil electrical parameters, and has a wider applicable frequency range [13] [20]. At the same time, the electric field at a general distance can only be solved through interpolation in the horizontal direction, without considering that the transmission line height is not on the differential grid. The traditional leapfrog differential format has been used to analyze the terminal response of overhead lines above dispersive soil excited by direct lightning strikes [21]. However, this format needs to meet Courant stability conditions [22], and it is difficult to directly analyze circuits with non-pure resistive terminal loads.

The main contribution of this paper is to propose a method with fully analytical equations and strong robustness that overcomes these difficulties. This method is based on the vector fitting (VF) method [23] recursive convolution, and implicit Wendroff (IW) difference format [24]. At the same time, the robustness of the method is enhanced by using integral by parts to process the convolution term to avoid the case where the denominator is 0.

The rest of this paper is organized as follows. Section II gives the governing equations of the solved indirect lightning coupling to overhead lines model. An iterative equation for solving the governing equations is derived in Section III. Section IV conducts verification and analysis. The conclusions are provided in Section V.

II. Indirect Lightning Coupling to Overhead Lines Model

A. Governing equations

The model of overhead lines excited by indirect lightning is shown in Fig. 1. There are two sets of coordinate systems in Fig.1, one of which is a Cartesian coordinate system (x-y-z) established with y=0 as the endpoint of the wire. The other is the cylindrical coordinate system (ρ-θ-z) established with the intersection of the lightning channel and the ground as the coordinate origin, whose coordinate origin can be expressed as $(-x_c, -y_c, 0)$ in the Cartesian coordinate system. The z in two coordinate systems has the same meaning.

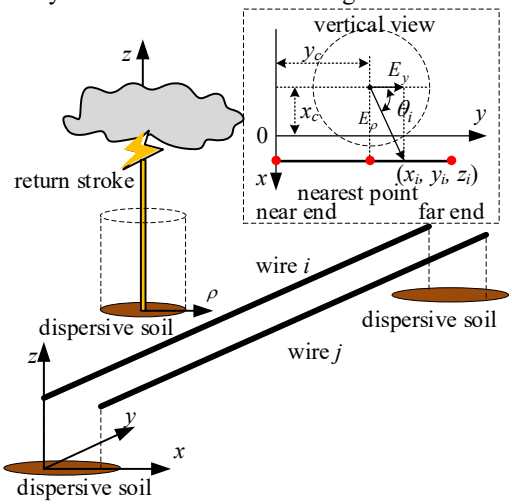

Fig. 1. Overhead lines excited by indirect lightning.

The gap between the overhead line and the ground is quite large, and it's filled with air, so we can ignore conductivity in our model [25]. The Agrawal form of the governing equations for N conductors with a length of l above the reference plane in the time domain is [26]:

$$\frac{\partial \boldsymbol{V}^s(t,y)}{\partial y}+\boldsymbol{L}\frac{\partial \boldsymbol{I}(t,y)}{\partial t}+\boldsymbol{\varsigma}(t)*\frac{\partial \boldsymbol{I}(t,y)}{\partial t}=\boldsymbol{E}_y^e(t,y) \tag{1}$$

$$\frac{\partial \boldsymbol{I}(t,y)}{\partial y}+\boldsymbol{C}\frac{\partial \boldsymbol{V}^s(t,y)}{\partial t}=\boldsymbol{0} \tag{2}$$

where * represents convolution, $\boldsymbol{V}^s$ and $\boldsymbol{I}$ are the scattered voltage and distributed current on the overhead lines, respectively. $\boldsymbol{E}_y^e$ denotes the longitudinal electric field along the overhead line direction. $\boldsymbol{L}$ is the inductance matrix generated by the time-variant magnetic field of adjacent wires. $\boldsymbol{\varsigma}(t)$ is related to ground impedance $\boldsymbol{Z}_g$ and is represented as

$$\boldsymbol{\varsigma}(f)=\frac{\boldsymbol{Z}_g(f)}{j\omega} \tag{3}$$

where f stands for the frequency, $\omega=2\pi f$ is the angular frequency. Compared with the ground impedance, the influence of internal resistance caused by skin effect on lightning induced voltage can be ignored [27], so it is not shown in (1).

Assuming that the center coordinates of any two wires i and j are (x_i, y_i, z_i) and (x_j, y_i, z_j), $y_i \in [0, l]$, $i,j=1, 2, \ldots, N$, respectively, with a distance of d_{ij}. The diagonal and non diagonal elements of ground impedance $\boldsymbol{Z}_g$ in the expression of Sunde [28] can be written as:

$$Z_{gii}(f)=\frac{j\omega\mu_0}{2\pi}\ln\left[\left(1+\gamma_g(f)z_i\right)\Big/\left(\gamma_g(f)z_i\right)\right] \tag{4}$$

$$Z_{gij}(f)=\frac{j\omega\mu_0}{4\pi}\ln\left[\frac{\left(1+\gamma_g(f)\frac{z_i+z_j}{2}\right)^2+\left(\gamma_g(f)\frac{d_{ij}}{2}\right)^2}{\left(\gamma_g(f)\frac{z_i+z_j}{2}\right)^2+\left(\gamma_g(f)\frac{d_{ij}}{2}\right)^2}\right] \tag{5}$$

TABLE 1. COEFFICIENTS OF THE LS SOIL MODEL [9].

k	1	2	3	4	5
a_k	3.4×10^6	2.74×10^5	2.58×10^4	3.38×10^3	526
k	6	7	8	9	10
a_k	133	27.2	12.5	4.8	2.17
k	11	12	13	—	—
a_k	0.98	0.392	0.173	—	—

where γ_g is the propagation constant of electromagnetic waves in the ground, which can be expressed as $\gamma_g^2(f)=j\omega\mu_0[\sigma_g(f)+j\omega\varepsilon_g(f)]$. Based on the LS soil model [9], soil electrical parameters for water percentage p are:

$$\sigma_g(f)=\sigma_0+2\pi\varepsilon_0\sum_{k=1}^{13}\frac{a_k f_k (f/f_k)^2}{1+(f/f_k)^2} \tag{6}$$

$$\varepsilon_g(f)=\varepsilon_0\varepsilon_\infty+\varepsilon_0\sum_{k=1}^{13}\frac{a_k}{1+(f/f_k)^2} \tag{7}$$

$$\sigma_0=8\left(p/10\right)^{1.54}\times10^{-3} \tag{8}$$

$$f_k=\left(p/10\right)^{1.28}\times10^{k-1} \tag{9}$$

where σ_0 (S/m) denotes the electrical conductivity of the soil at 100 Hz, and coefficient ε_∞ is 5. The magnetic permeability of the air is $\mu_0=4\pi\times10^{-7}$ (H/m). The range of frequency f is 0 to 5 MHz, and the range of soil water percentage p is 0.2% to 30%. The coefficient a_k is shown in Table 1.

The $\varsigma(f)$ contains frequency dependent parameters, making it difficult to directly obtain the analytical form in the time domain. Combined with VF method [23], $\varsigma(f)$ can be written as

$$\varsigma(f)=\sum_{m=1}^{N_{VF}}\frac{\boldsymbol{b}_m}{j\omega-a_m} \tag{10}$$

where N_{VF} is the number of residues. a_m and $\boldsymbol{b}_m$ are poles and residues respectively, m=1, 2, …, N_{VF}. Converting (10) to the time domain is expressed as:

$$\varsigma(t)=\sum_{m=1}^{N_{VF}}\boldsymbol{b}_m\exp\left(a_m t\right) \tag{11}$$

B. Solution of Indirect lightning electromagnetic field

The EMF generated by lightning is rotationally symmetric about the z-axis, and any ρ-z plane is equivalent. Therefore, the lightning EMF can be solved in a 2D coordinate system. As shown in Fig. 2, for any rotating cross section, the outer layer of the solution domain (soil and air) is CMPL, and lightning is used as the boundary condition on the left. The iterative equations for solving the electric field considering the LS soil model are shown in the Appendix, which is based on the Debye representation of frequency dependence ground [20]. It can be known from the previous analysis that the CPML boundary condition has nothing to do with the medium and can be effectively used in dispersive soil.

By observing the two coordinate systems in Fig.1, it can be obtained that the longitudinal electric field component of the lightning at any point (x_i, y_i, z_i) on the overhead lines along the direction of the transmission line is:

$$E_y=E_\rho(\rho=\rho_i,\theta=\theta_i,z=z_i)\cdot\cos\theta_i \tag{12}$$

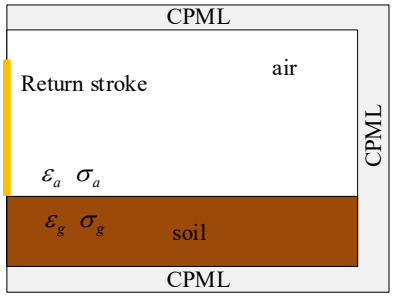

Fig. 2. Solution region of lightning electromagnetic field.

$$\cos\theta_i=(y_i-y_c)/\rho_i \tag{13}$$

$$\rho_i=\sqrt{\left(x_c+x_i\right)^2+(y_i-y_c)^2} \tag{14}$$

When the position of the overhead lines is not on the differential grid of the lightning horizontal electric field, one-dimensional interpolation can be performed on the nearby differential grid [10]. In order to avoid being limited by the time and space segments of lightning EMFs, a 2D cubic spline interpolation method is used to solve the vertical electric field at any position and time on the overhead lines based on the mapping relationship among distance, time and vertical electric field. The interpolation method can be easily implemented in MATLAB. Whether interpolation is used or not, the larger the grid spacing, the lower the accuracy of the solution results.

III. SOLUTION OF TIME-DOMAIN GOVERNING EQUATIONS

The time-domain governing equation (1) contains the convolution of current $\boldsymbol{I}$, which is the key point for their solution.

The schematic diagram of the improved IW differential grid is shown in Fig. 3. The wire is divided into NY segments, each with a length of Δy. The subscript of the variable name indicates space along the direction of the overhead lines, and the superscript represents time. The hollow circle in the middle is the actual solution position. The total time is divided into NT segments, with each segment being Δt.

At time $t=n\Delta t$, n=0, 1, …, NT, substituting (11) into the convolution item in (1) can get

$$\varsigma(t)*\frac{\partial \boldsymbol{I}(t,y)}{\partial t}=\int_0^{n\Delta t}\sum_{m=1}^{N_{VF}}\boldsymbol{b}_m\exp\left[a_m\left(n\Delta t-\tau\right)\right]\frac{\mathrm{d}\boldsymbol{I}(\tau,y)}{\mathrm{d}\tau}\mathrm{d}\tau \tag{15}$$

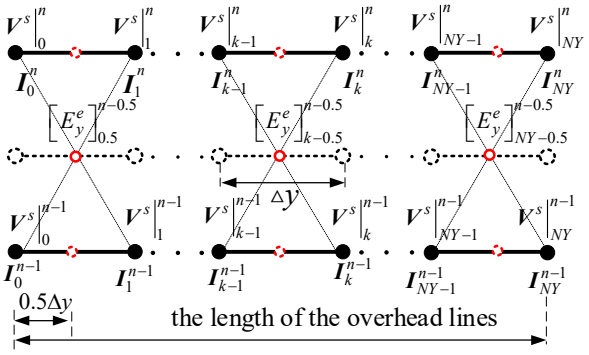

Fig. 3. Improved IW differential grid of overhead lines excited by lightning.

Let the right side of (15) be equal to $\sum_{m=1}^{N_{VF}} \boldsymbol{\psi}_m\big|_y^n$. Then

$$\boldsymbol{\psi}_m\big|_y^n = \exp\left(a_m \Delta t\right)\boldsymbol{\psi}_m\big|_y^{n-1} + \int_{(n-1)\Delta t}^{n\Delta t} \boldsymbol{b}_m \exp\left[a_m\left(n\Delta t - \tau\right)\right]\frac{\mathrm{d}\boldsymbol{I}(\tau, y)}{\mathrm{d}\tau}\mathrm{d}\tau \quad (16)$$

$$\boldsymbol{\psi}_m\big|_y^n = \exp\left(a_m \Delta t\right)\boldsymbol{\psi}_m\big|_y^{n-1} + \boldsymbol{\varphi}_m\big|_y^n \quad (17)$$

where

$$\boldsymbol{\varphi}_m\big|_y^n = \boldsymbol{b}_m \exp\left(n a_m \Delta t\right)\cdot\int_{(n-1)\Delta t}^{n\Delta t} \exp\left(-a_m \tau\right)\mathrm{d}\boldsymbol{I}\left(\tau, y\right) \quad (18)$$

Using the integration by parts method, we can get,

$$\boldsymbol{\varphi}_m\big|_y^n = \boldsymbol{b}_m \boldsymbol{I}_y^n - \exp\left(a_m \Delta t\right)\boldsymbol{b}_m \boldsymbol{I}_y^{n-1} + \exp\left(n a_m \Delta t\right) a_m \boldsymbol{b}_m \int_{(n-1)\Delta t}^{n\Delta t} \exp\left(-a_m \tau\right)\boldsymbol{I}\left(\tau, y\right)\mathrm{d}\tau \quad (19)$$

Combined with the IW difference format [24], at spatial position $y=(k+0.5)\Delta y$, $k=0,1,\ldots, NY-1$, (19) can be simplified as:

$$\boldsymbol{\varphi}_m\big|_{k+0.5}^n = \boldsymbol{c}_m\left(\boldsymbol{I}_k^n + \boldsymbol{I}_{k+1}^n\right) - \boldsymbol{c}_m\left(\boldsymbol{I}_k^{n-1} + \boldsymbol{I}_{k+1}^{n-1}\right) \quad (20)$$

$$\boldsymbol{c}_m = 0.25\left[\exp\left(a_m \Delta t\right) + 1\right]\boldsymbol{b}_m \quad (21)$$

The result a_m in (20) and (21) does not appear independently in the denominator, so there is no need to discuss the case where $a_m=0$, and a more general solution is applicable. However, if the differential solution is directly performed, a_m will appear separately in the denominator [5] [21].

Therefore, combined with (17), the convolution part (15) can be written as:

$$\sum_{m=1}^{N_{VF}}\left[\boldsymbol{\psi}_m\right]_{k+0.5}^n = \boldsymbol{B}_a \bar{\boldsymbol{\psi}}_{k+1}^{n-1} + \boldsymbol{B}_b\left(\boldsymbol{I}_k^n + \boldsymbol{I}_{k+1}^n\right) - \boldsymbol{B}_b\left(\boldsymbol{I}_k^{n-1} + \boldsymbol{I}_{k+1}^{n-1}\right) \quad (22)$$

$$\bar{\boldsymbol{\psi}}_{k+1}^n = \underbrace{\left\{\left[\boldsymbol{\psi}_1, \boldsymbol{\psi}_2, \boldsymbol{\psi}_{N_{VF}}\right]_{k+0.5}^n\right\}^T}_{N_{VF}N\times 1} \quad (23)$$

$$\boldsymbol{B}_a = \underbrace{\left[\exp(a_1\Delta t)\boldsymbol{E}, \exp(a_2\Delta t)\boldsymbol{E}, \ldots, \exp(a_{N_{VF}}\Delta t)\boldsymbol{E}\right]}_{N\times N_{VF}N} \quad (24)$$

$$\boldsymbol{B}_b = \sum_{m=1}^{N_{VF}} \boldsymbol{c}_m \quad (25)$$

where $\boldsymbol{E}$ represents the N-order identity matrix, and T denotes the transposition of the matrix.

The scattered voltage and current can be expressed in vector form as:

$$\boldsymbol{W} = \underbrace{\left[\boldsymbol{V}_0^s, \boldsymbol{V}_1^s \ldots, \boldsymbol{V}_{NY}^s, \boldsymbol{I}_0, \boldsymbol{I}_1 \ldots, \boldsymbol{I}_{NY}\right]^T}_{2(NY+1)N\times 1} \quad (26)$$

The matrix form of (17) and (22)-(25) is:

$$\boldsymbol{\phi}^n = \boldsymbol{K}_a \boldsymbol{\phi}^{n-1} + \boldsymbol{K}_b \boldsymbol{W}^n - \boldsymbol{K}_b \boldsymbol{W}^{n-1} \quad (27)$$

where($\mathbf{0}$ represents the N-order zeros matrix)

$$\boldsymbol{A}_a = \underbrace{\begin{bmatrix} \exp(a_1\Delta t)\boldsymbol{E} & \mathbf{0} & \cdots & \mathbf{0} \\ \mathbf{0} & \exp(a_2\Delta t)\boldsymbol{E} & \ddots & \vdots \\ \vdots & \ddots & \ddots & \mathbf{0} \\ \mathbf{0} & \cdots & \mathbf{0} & \exp(a_{N_{VF}}\Delta t)\boldsymbol{E} \end{bmatrix}}_{N_{VF}N\times N_{VF}N} \quad (28)$$

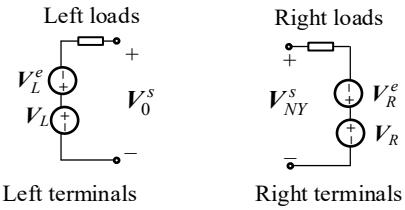

Fig. 4. Thevenin equivalent circuit of overhead line terminal.

$$\boldsymbol{K}_a = \underbrace{\begin{bmatrix} \boldsymbol{A}_a & \mathbf{0} & \cdots & \mathbf{0} \\ \mathbf{0} & \boldsymbol{A}_a & \ddots & \vdots \\ \vdots & \ddots & \ddots & \mathbf{0} \\ \mathbf{0} & \cdots & \mathbf{0} & \boldsymbol{A}_a \end{bmatrix}}_{(NY)N_{VF}N\times(NY)N_{VF}N} \quad (29)$$

$$\boldsymbol{A}_b = \underbrace{\left[\boldsymbol{c}_1, \boldsymbol{c}_2, \ldots, \boldsymbol{c}_{N_{VF}}\right]^T}_{N_{VF}N\times N} \quad (30)$$

$$\boldsymbol{K}_b = \underbrace{\begin{bmatrix} \mathbf{0} & \cdots & \mathbf{0} & \boldsymbol{A}_b & \boldsymbol{A}_b & \mathbf{0} & \cdots & \mathbf{0} \\ \mathbf{0} & \mathbf{0} & \cdots & \mathbf{0} & \boldsymbol{A}_b & \boldsymbol{A}_b & \ddots & \vdots \\ \vdots & \vdots & \vdots & \vdots & \ddots & \ddots & \ddots & \mathbf{0} \\ \mathbf{0} & \mathbf{0} & \mathbf{0} & \mathbf{0} & \cdots & \mathbf{0} & \boldsymbol{A}_b & \boldsymbol{A}_b \end{bmatrix}}_{(NY)N_{VF}N\times 2(NY+1)N} \quad (31)$$

$$\boldsymbol{\phi} = \underbrace{\left[\bar{\boldsymbol{\psi}}_1, \bar{\boldsymbol{\psi}}_2, \ldots, \bar{\boldsymbol{\psi}}_{NY}\right]^T}_{(NY)N_{VF}N\times 1} \quad (32)$$

Combining (1), (2) and (22), the IW difference format for the time domain governing equations can be written as:

$$\frac{1}{2\Delta y}\left(\boldsymbol{V}^s\big|_{k+1}^n - \boldsymbol{V}^s\big|_k^n + \boldsymbol{V}^s\big|_{k+1}^{n-1} - \boldsymbol{V}^s\big|_k^{n-1}\right) + \frac{\boldsymbol{L}}{2\Delta t}\left(\boldsymbol{I}_k^n - \boldsymbol{I}_k^{n-1} + \boldsymbol{I}_{k+1}^n - \boldsymbol{I}_{k+1}^{n-1}\right) + \sum_{m=1}^{N_{VF}}\boldsymbol{\psi}_m\big|_{k+0.5}^n = \boldsymbol{E}_y^e\big|_{k+0.5}^{n-0.5} \quad (33)$$

$$\frac{1}{2\Delta y}\left(\boldsymbol{I}_{k+1}^n - \boldsymbol{I}_k^n + \boldsymbol{I}_{k+1}^{n-1} - \boldsymbol{I}_k^{n-1}\right) + \frac{\boldsymbol{C}}{2\Delta t}\left(\boldsymbol{V}^s\big|_{k+1}^n - \boldsymbol{V}^s\big|_{k+1}^{n-1} + \boldsymbol{V}^s\big|_k^n - \boldsymbol{V}^s\big|_k^{n-1}\right) = \mathbf{0} \quad (34)$$

Simplify to:

$$\boldsymbol{V}^s\big|_k^n - \boldsymbol{V}^s\big|_{k+1}^n - \frac{\Delta y}{\Delta t}\boldsymbol{L}\left(\boldsymbol{I}_k^n + \boldsymbol{I}_{k+1}^n\right) = -\boldsymbol{V}^s\big|_k^{n-1} + \boldsymbol{V}^s\big|_{k+1}^{n-1} - \frac{\Delta y}{\Delta t}\boldsymbol{L}\left(\boldsymbol{I}_k^{n-1} + \boldsymbol{I}_{k+1}^{n-1}\right) - 2\Delta y\,\boldsymbol{E}_y^e\big|_{k+0.5}^{n-0.5} + 2\Delta y\sum_{m=1}^{N_{VF}}\boldsymbol{\psi}_m\big|_{k+0.5}^n \quad (35)$$

$$-\frac{\Delta y}{\Delta t}\boldsymbol{C}\left(\boldsymbol{V}^s\big|_k^n + \boldsymbol{V}^s\big|_{k+1}^n\right) + \boldsymbol{I}_k^n - \boldsymbol{I}_{k+1}^n = -\frac{\Delta y}{\Delta t}\boldsymbol{C}\left(\boldsymbol{V}^s\big|_k^{n-1} + \boldsymbol{V}^s\big|_{k+1}^{n-1}\right) - \boldsymbol{I}_k^{n-1} + \boldsymbol{I}_{k+1}^{n-1} \quad (36)$$

In the Thevenin terminal equivalent circuit shown in Fig. 4, $\boldsymbol{V}_L^e$ and $\boldsymbol{V}_R^e$ are the equivalent voltages of the transverse electric field perpendicular to the ground at the left and right ends of the overhead lines, respectively, and $\boldsymbol{V}_L$, $\boldsymbol{V}_R$ and $\boldsymbol{Z}_L$, $\boldsymbol{Z}_R$ represent the lumped voltage power sources and loads at both ends.

Assuming that both ends are resistance series inductance loads (R-L), specifically R_L, L_L and R_R, L_R, which are also the most

common terminal loads in power systems. According to Kirchhoff's voltage law, the terminal circuit relationship is:

$$\boldsymbol{V}_0^s = \boldsymbol{V}_L - \left(\boldsymbol{R}_L \boldsymbol{I}_0 + \boldsymbol{L}_L \frac{\partial \boldsymbol{I}_0}{\partial t} \right) - \boldsymbol{V}_L^e \tag{37}$$

$$\boldsymbol{V}_{NY}^s = \boldsymbol{V}_R + \left(\boldsymbol{R}_R \boldsymbol{I}_{NY} + \boldsymbol{L}_R \frac{\partial \boldsymbol{I}_{NY}}{\partial t} \right) - \boldsymbol{V}_R^e \tag{38}$$

Combined with the backward difference technique, and simplified to:

$$\boldsymbol{V}^s\big|_0^n + \left(\boldsymbol{R}_L + \boldsymbol{L}_L/\Delta t\right)\boldsymbol{I}_0^n = \boldsymbol{L}_L/\Delta t\, \boldsymbol{I}_0^{n-1} + \boldsymbol{V}_L^n - \boldsymbol{V}_L^{e,n} \tag{39}$$

$$\boldsymbol{V}^s\big|_{NY}^n - \left(\boldsymbol{R}_R + \boldsymbol{L}_R/\Delta t\right)\boldsymbol{I}_{NY}^n = -\boldsymbol{L}_R/\Delta t\, \boldsymbol{I}_{NY}^{n-1} + \boldsymbol{V}_R^n - \boldsymbol{V}_R^{e,n} \tag{40}$$

Similarly, if the load at both ends is a parallel load of resistance and capacitance (*R*-*C*), specifically R_L, C_L and R_R, C_R. According to Kirchhoff's current law and combined with backward differential technology, the terminal circuit relationship is simplified as:

$$\begin{aligned}&\left(\boldsymbol{R}_L^{-1} + \boldsymbol{C}_L/\Delta t\right)\boldsymbol{V}^s\big|_0^n + \boldsymbol{I}_0^n = \boldsymbol{C}_L/\Delta t\, \boldsymbol{V}^s\big|_0^{n-1} \\ &+\left(\boldsymbol{R}_L^{-1} + \boldsymbol{C}_L/\Delta t\right)\left(\boldsymbol{V}_L^n - \boldsymbol{V}_L^{e,n}\right) - \boldsymbol{C}_L/\Delta t\left(\boldsymbol{V}_L^{n-1} - \boldsymbol{V}_L^{e,n-1}\right)\end{aligned} \tag{41}$$

$$\begin{aligned}&\left(\boldsymbol{R}_R^{-1} + \boldsymbol{C}_R/\Delta t\right)\boldsymbol{V}^s\big|_{NY}^n - \boldsymbol{I}_{NY}^n = \boldsymbol{C}_R/\Delta t\, \boldsymbol{V}^s\big|_{NY}^{n-1} \\ &+\left(\boldsymbol{R}_R^{-1} + \boldsymbol{C}_R/\Delta t\right)\left(\boldsymbol{V}_R^n - \boldsymbol{V}_R^{e,n}\right) - \boldsymbol{C}_R/\Delta t\left(\boldsymbol{V}_R^{n-1} - \boldsymbol{V}_R^{e,n-1}\right)\end{aligned} \tag{42}$$

Representing (35), (36), (39)- (42) in matrix form, the iterative equation is:

$$\boldsymbol{W}^n = \boldsymbol{A}^{-1} \cdot \left[\boldsymbol{B}\boldsymbol{W}^{n-1} + \boldsymbol{D}_1^n + \boldsymbol{D}_2^{n-1} - 2\Delta y(\boldsymbol{F}^{n-0.5} - \boldsymbol{K}\boldsymbol{\phi}^{n-1}) \right] \tag{43}$$

where the coefficients are:

$$\boldsymbol{A}_v = -\Delta y/\Delta t\, \boldsymbol{L} - 2\Delta y \boldsymbol{B}_b \tag{44}$$

$$\boldsymbol{A}_i = -\Delta y/\Delta t\, \boldsymbol{C} \tag{45}$$

$$\boldsymbol{A} = \underbrace{\begin{bmatrix} \boldsymbol{E} & -\boldsymbol{E} & \cdots & \boldsymbol{0} & \boldsymbol{0} & \boldsymbol{A}_v & \boldsymbol{A}_v & \cdots & \boldsymbol{0} & \boldsymbol{0} \\ \boldsymbol{0} & \boldsymbol{E} & \cdots & \boldsymbol{0} & \boldsymbol{0} & \boldsymbol{0} & \boldsymbol{A}_v & \cdots & \boldsymbol{0} & \boldsymbol{0} \\ \vdots & \vdots & \vdots & \vdots & \vdots & \vdots & \vdots & \vdots & \vdots & \vdots \\ \boldsymbol{0} & \boldsymbol{0} & \cdots & \boldsymbol{E} & -\boldsymbol{E} & \boldsymbol{0} & 0 & \cdots & \boldsymbol{A}_v & \boldsymbol{A}_v \\ \boldsymbol{A}_i & \boldsymbol{A}_i & \cdots & \boldsymbol{0} & \boldsymbol{0} & \boldsymbol{E} & -\boldsymbol{E} & \cdots & \boldsymbol{0} & \boldsymbol{0} \\ \boldsymbol{0} & \boldsymbol{A}_i & \cdots & \boldsymbol{0} & \boldsymbol{0} & \boldsymbol{0} & \boldsymbol{E} & \cdots & \boldsymbol{0} & \boldsymbol{0} \\ \vdots & \vdots & \vdots & \vdots & \vdots & \vdots & \vdots & \vdots & \vdots & \vdots \\ \boldsymbol{0} & \boldsymbol{0} & \cdots & \boldsymbol{A}_i & \boldsymbol{A}_i & \boldsymbol{0} & \boldsymbol{0} & \cdots & \boldsymbol{E} & -\boldsymbol{E} \\ \boldsymbol{Z}_{L11} & \boldsymbol{0} & \cdots & \boldsymbol{0} & \boldsymbol{0} & \boldsymbol{Z}_{L12} & \boldsymbol{0} & \cdots & \boldsymbol{0} & \boldsymbol{0} \\ \boldsymbol{0} & \boldsymbol{0} & \cdots & \boldsymbol{0} & \boldsymbol{Z}_{R11} & \boldsymbol{0} & \boldsymbol{0} & \cdots & \boldsymbol{0} & \boldsymbol{Z}_{R12} \end{bmatrix}}_{2(NY+1)N \times 2(NY+1)N} \tag{46}$$

$$\boldsymbol{B} = \underbrace{\begin{bmatrix} -\boldsymbol{E} & \boldsymbol{E} & \cdots & \boldsymbol{0} & \boldsymbol{0} & \boldsymbol{A}_v & \boldsymbol{A}_v & \cdots & \boldsymbol{0} & \boldsymbol{0} \\ \boldsymbol{0} & -\boldsymbol{E} & \cdots & \boldsymbol{0} & \boldsymbol{0} & \boldsymbol{0} & \boldsymbol{A}_v & \cdots & \boldsymbol{0} & \boldsymbol{0} \\ \vdots & \vdots & \vdots & \vdots & \vdots & \vdots & \vdots & \vdots & \vdots & \vdots \\ \boldsymbol{0} & \boldsymbol{0} & \cdots & -\boldsymbol{E} & \boldsymbol{E} & \boldsymbol{0} & \boldsymbol{0} & \cdots & \boldsymbol{A}_v & \boldsymbol{A}_v \\ \boldsymbol{A}_i & \boldsymbol{A}_i & \cdots & \boldsymbol{0} & \boldsymbol{0} & -\boldsymbol{E} & \boldsymbol{E} & \cdots & \boldsymbol{0} & \boldsymbol{0} \\ \boldsymbol{0} & \boldsymbol{A}_i & \cdots & \boldsymbol{0} & \boldsymbol{0} & \boldsymbol{0} & -\boldsymbol{E} & \cdots & \boldsymbol{0} & \boldsymbol{0} \\ \vdots & \vdots & \vdots & \vdots & \vdots & \vdots & \vdots & \vdots & \vdots & \vdots \\ \boldsymbol{0} & \boldsymbol{0} & \cdots & \boldsymbol{A}_i & \boldsymbol{A}_i & \boldsymbol{0} & \boldsymbol{0} & \cdots & -\boldsymbol{E} & -\boldsymbol{E} \\ \boldsymbol{Z}_{L21} & \boldsymbol{0} & \cdots & \boldsymbol{0} & \boldsymbol{0} & \boldsymbol{Z}_{L22} & \boldsymbol{0} & \cdots & \boldsymbol{0} & \boldsymbol{0} \\ \boldsymbol{0} & \boldsymbol{0} & \cdots & \boldsymbol{0} & \boldsymbol{Z}_{R21} & \boldsymbol{0} & \boldsymbol{0} & \cdots & \boldsymbol{0} & \boldsymbol{Z}_{R22} \end{bmatrix}}_{2(NY+1)N \times 2(NY+1)N} \tag{47}$$

$$\boldsymbol{D}_1 = \underbrace{\left[\boldsymbol{0}, \boldsymbol{0}, \ldots, \boldsymbol{0}, \boldsymbol{I}_{eqL1}, \boldsymbol{I}_{eqR1}\right]^T}_{2(NY+1)N \times 1} \tag{48}$$

$$\boldsymbol{D}_2 = \underbrace{\left[\boldsymbol{0}, \boldsymbol{0}, \ldots, \boldsymbol{0}, \boldsymbol{I}_{eqL2}, \boldsymbol{I}_{eqR2}\right]^T}_{2(NY+1)N \times 1} \tag{49}$$

$$\boldsymbol{F} = \underbrace{\left[\left[\boldsymbol{E}_y^e\right]_{0.5}, \left[\boldsymbol{E}_y^e\right]_{1.5}, \ldots, \left[\boldsymbol{E}_y^e\right]_{NY-0.5}, \boldsymbol{0}, \ldots, \boldsymbol{0}\right]^T}_{2(NY+1)N \times 1} \tag{50}$$

$$\boldsymbol{K} = \underbrace{\begin{bmatrix} \boldsymbol{B}_a & \boldsymbol{0} & \cdots & \boldsymbol{0} \\ \boldsymbol{0} & \boldsymbol{B}_a & \ddots & \vdots \\ \vdots & \ddots & \ddots & \boldsymbol{0} \\ \boldsymbol{0} & \cdots & \boldsymbol{0} & \boldsymbol{B}_a \\ \vdots & \vdots & \vdots & \vdots \\ \boldsymbol{0} & \cdots & \boldsymbol{0} & \boldsymbol{0} \end{bmatrix}}_{2(NY+1)N \times (NY)N_{YF}N} \tag{51}$$

where $\boldsymbol{I}_{eqL1}$, $\boldsymbol{I}_{eqR1}$, $\boldsymbol{I}_{eqL2}$ and $\boldsymbol{I}_{eqR2}$ are the equivalent sources of the terminal circuit and the transverse electric field, and the specific values are shown in Fig.5. When the terminal Thevenin equivalent circuit is *R*-*L* or *R*-*C* load, the remaining coefficients of (46) and (47) are shown in Fig.5. When the loads of overhead lines are of different types, modifying according to the rules in Fig. 5 can obtain loads of any arrangement type, thus achieving the solution of hybrid terminal load circuits.

$\boldsymbol{Z}_{L11} = \boldsymbol{E}$ $\boldsymbol{Z}_{L12} = \boldsymbol{R}_L + \boldsymbol{L}_L/\Delta t$ $\boldsymbol{Z}_{L21} = \boldsymbol{0}$ $\boldsymbol{Z}_{L22} = \boldsymbol{L}_L/\Delta t$ $\boldsymbol{I}_{eqL1} = \boldsymbol{V}_L - \boldsymbol{V}_L^e$ $\boldsymbol{I}_{eqL2} = \boldsymbol{0}$ Left(*R*-*L* loads)	$\boldsymbol{Z}_{L11} = \boldsymbol{R}_L^{-1} + \boldsymbol{C}_L/\Delta t$ $\boldsymbol{Z}_{L12} = \boldsymbol{E}$ $\boldsymbol{Z}_{L21} = \boldsymbol{C}_L/\Delta t$ $\boldsymbol{Z}_{L22} = \boldsymbol{0}$ $\boldsymbol{I}_{eqL1} = \boldsymbol{Z}_{L11}(\boldsymbol{V}_L^n - \boldsymbol{V}_L^e)$ $\boldsymbol{I}_{eqL2} = -\boldsymbol{Z}_{L21}(\boldsymbol{V}_L - \boldsymbol{V}_L^e)$ Left(*R*-*C* loads)
$\boldsymbol{Z}_{R11} = \boldsymbol{E}$ $\boldsymbol{Z}_{R12} = -\boldsymbol{R}_R - \boldsymbol{L}_R/\Delta t$ $\boldsymbol{Z}_{R21} = \boldsymbol{0}$ $\boldsymbol{Z}_{R22} = -\boldsymbol{L}_R/\Delta t$ $\boldsymbol{I}_{eqR1} = \boldsymbol{V}_R - \boldsymbol{V}_R^e$ $\boldsymbol{I}_{eqR2} = \boldsymbol{0}$ Right (*R*-*L* loads)	$\boldsymbol{Z}_{R11} = \boldsymbol{R}_R^{-1} + \boldsymbol{C}_R/\Delta t$ $\boldsymbol{Z}_{R12} = -\boldsymbol{E}$ $\boldsymbol{Z}_{R21} = \boldsymbol{C}_R/\Delta t$ $\boldsymbol{Z}_{R22} = \boldsymbol{0}$ $\boldsymbol{I}_{eqR1} = \boldsymbol{Z}_{R11}(\boldsymbol{V}_R^n - \boldsymbol{V}_R^e)$ $\boldsymbol{I}_{eqR2} = -\boldsymbol{Z}_{R21}(\boldsymbol{V}_R - \boldsymbol{V}_R^e)$ Right (*R*-*C* loads)

Fig.5. Coefficients when the left and right terminal Thevenin equivalent circuits are *R*-*C* parallel or *R*-*L* series loads.

IV. Experiment and Verification

In order to verify the proposed method, the modified transmission line model with linear current decay（MTLL）lightning model [29] is selected as the excitation model, and the current of the lightning channel can be expressed as:

$$i(z,t) = (1 - z/H)i(0, t - z/v), \quad t \geq z/v \tag{52}$$

where H represents the length of the lightning channel, which is taken as 7500 m in this paper, and the lightning return velocity v is 1.5×10^8 m/s。

The FRS has a larger amplitude than the SRS, and the SRS has more high-frequency energy, all of which have good representativeness. Both cases are therefore analyzed in this paper. The base current of the lightning channel represents the sum of two Heidler functions:

TABLE 2. PARAMETERS OF THE FIRST- AND SUBSEQUENT- RETURN STROKE.

parameters	I_{01} (kA)	τ_{11} (μs)	τ_{12} (μs)	n_1	I_{02} (kA)	τ_{21} (μs)	τ_{22} (μs)	n_2
FRS	28	1.8	95	2	-	-	-	-
SRS	10.7	0.25	2.5	2	6.5	2.1	230	2

$$i(0,t)=\frac{I_{01}}{\eta_1}\frac{(t/\tau_{11})^{n_1}}{1+(t/\tau_{11})^{n_1}}e^{-\frac{t}{\tau_{12}}}+\frac{I_{02}}{\eta_2}\frac{(t/\tau_{21})^{n_2}}{1+(t/\tau_{21})^{n_2}}e^{-\frac{t}{\tau_{22}}} \quad (53)$$

$$\eta_1=\exp\left[-(\tau_{11}/\tau_{12})\cdot(n_1\tau_{12}/\tau_{11})^{(1/n_1)}\right] \quad (54)$$

$$\eta_2=\exp\left[-(\tau_{21}/\tau_{22})\cdot(n_2\tau_{22}/\tau_{21})^{(1/n_2)}\right] \quad (55)$$

where coefficients of the FRS and the SRS are shown in Table 2 [30].

The geometric parameters of a typical 35 kV three-phase overhead lines are shown in Fig.6. The origin of the coordinates is the midpoint of the bottom of the pole. The total length of the transmission line is 5 km, and the lightning strike point is selected as 2 km, located on the side of the coordinate phase A, and the coordinates of the lightning strike point are x=−50 m, y=2 km, z=0. Assuming the thickness of the soil is 500m.

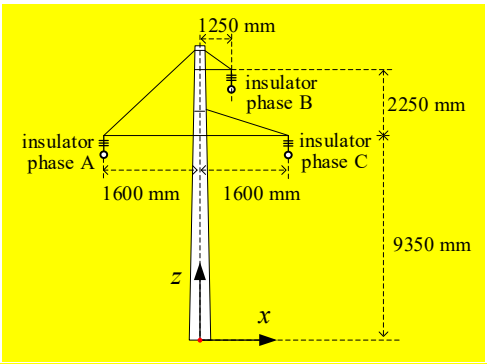

Fig. 6. Geometric relationship of a 35kV three-phase transmission lines without ground wire.

A. Performance of the proposed method

The case where the soil water percentage is set to p=0.2, 1, 2, 5, 10, and 30 is selected for validation as it will be used later. The variations in soil electrical parameters with different water percentages are illustrated in Fig. 7. In general, as the water percentage increases, conductivity tends to rise, while the dielectric constant tends to decrease and becomes more sensitive to changes in frequency. At higher frequencies, the difference in the dielectric constant of soil with different water percentages gradually diminishes.

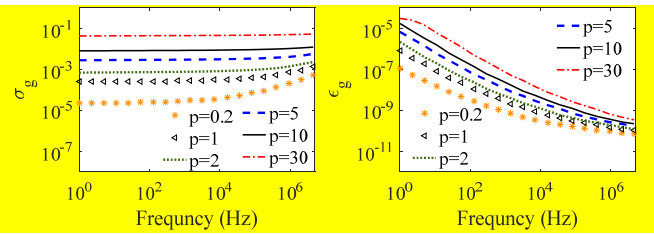

Fig.7. Conductivity σ_g and dielectric constant ε_g of the soil at different water percentages.

The VF accuracy of ground impedance related quantity $\varsigma(f)$ directly affects the performance of the proposed method. Actually, the value of $j\omega\varsigma(f)$ is the ground impedance $\boldsymbol{Z}_g$ in this paper. The main diagonal element $\boldsymbol{Z}_{g11}$ and the non-main diagonal element $\boldsymbol{Z}_{g12}$ of the ground impedance matrix value are selected for verification, and the results are shown in Fig.8. The comparison shows that the calculation results of the VF method are consistent with the real values.

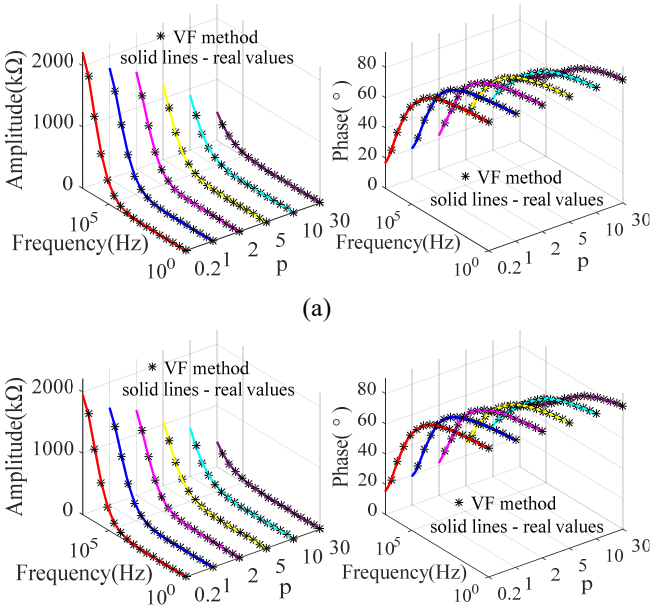

Fig.8. The ground impedance of the analyzed overhead lines model under different soil water percentages: (a) Z_{g11}; (b) Z_{g12}.

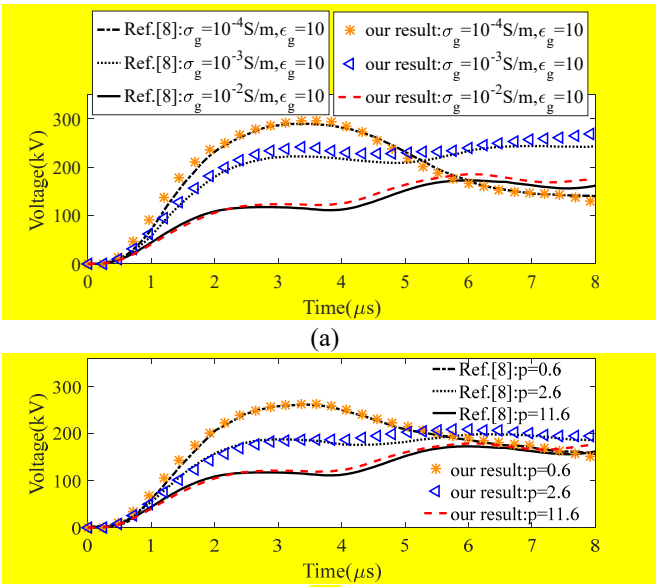

Fig.9. Comparison of coupling voltage of the overhead line with a length of 1000 m and a height of 10 m, when the soil electrical parameters are: (a) constant; (b) frequency-dependent.

We validate our method by comparing it with the results of Akbari et al. [8], as shown in Fig. 9. Fig.9 (a) represents the case of constant electrical parameters, while Fig. 9(b) illustrates the case involving dispersive soil employing the LS model. Under the conditions of constant soil electrical parameters, the iterative formula of our method for the lightning EMFs in air and soil will be simplified to the formula in [15]. We adopt the same parameters as in [8]. The length of the overhead line is 1000 m, and the lightning channel of the FRS is equidistant from both ends of the overhead line, and the nearest point distance is 50m. Reference [8] adopts the COMSOL base on the FEM method working in the frequency domain and achieves time-domain solution through numerical inverse Fourier transform. There are slight differences between the two methods in Fig.9, which may be due to the use of numerical inverse Fourier transform.

All validations were conducted on computers equipped with Intel i7 with 16 GB RAM. In the case where the COMSOL simulation involves 104019 spatial elements and 1000 frequency points, it requires about 50 min of solving time and 2.17 GB of storage (including memory allocation for modeling). In solving lightning EMFs, employing 1000 time points and 257075 spatial points, our method requires 22 s for completion. In the context of solving the governing equations (1) and (2) with 107500 points to be computed, it takes 1.03s. In total, the entire solution process for the proposed method takes around 23 s, with a maximum peak memory usage of 31.9 MB. Considering both memory and time consumption, it is evident that the proposed method outperforms COMSOL.

B. Coupling voltage for different types of loads

The terminals of the power system are usually inductive components, so the terminal Thevenin equivalent circuit can be connected in series with *R-L* loads. However, to ensure stable and reliable operation of the power system, the power factor is always around 1. As a large number of new energy vehicles are connected to the grid, the capacitive load in the power system is also increasing, and the terminal load can be equivalent to an *R-C* parallel circuit. We are interested in the impact of indirect lightning on the terminal circuit, so we will only discuss the coupling value at the both ends. It takes a certain amount of time for the lightning electromagnetic energy to reach both ends, so in the subsequent verification, the results of 0-5μs will not be displayed. In order to easily show the effects of different load types, a soil water percentage p=1 is randomly selected for verification.

Assuming that the two ends of the three-phase overhead lines are connected to the same load, the load includes three situations, case 1: 500 Ω pure resistance loads (power factor 1), case 2: 500 Ω and 0.22 H resistance series inductance loads (power factor 0.90), case 3: 500 Ω and 0.90 μF resistance parallel capacitance loads (power factor −0.99). The coupling results of the overhead lines excited by the FRS and the SRS are shown in Fig.10 and Fig.11. Regardless of the FRS or the SRS, compared with the *R* loads, the *R-L* loads increases the coupling voltage value, while the *R-C* loads significantly reduce the coupling voltage value. The reason is that both capacitive loads and inductive loads have energy storage properties. Capacitive loads will hinder voltage changes, whereas inductive loads will not hinder voltage changes, but will hinder current changes, as shown in Fig. 12 and Fig. 13.

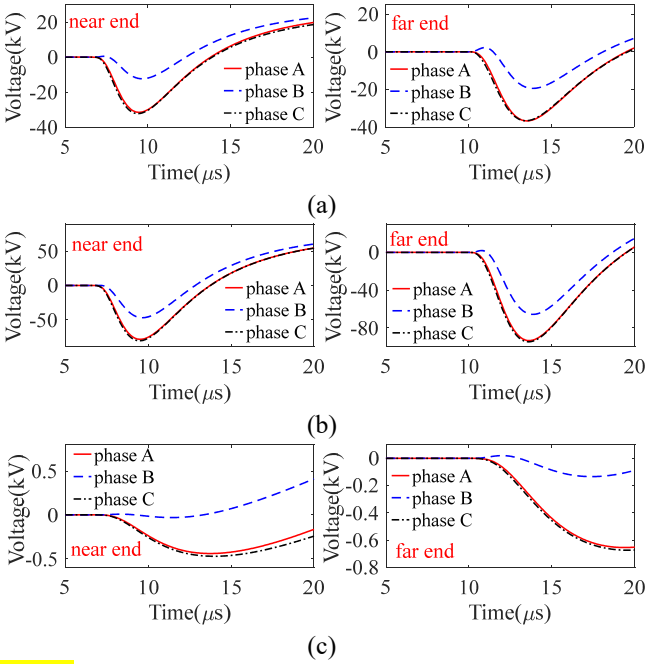

Fig. 10. When *p*=1, the coupling voltage at both ends on the overhead lines with different terminal loads excited by the FRS: (a) *R* loads; (b) *R-L* loads; (c) *R-C* loads.

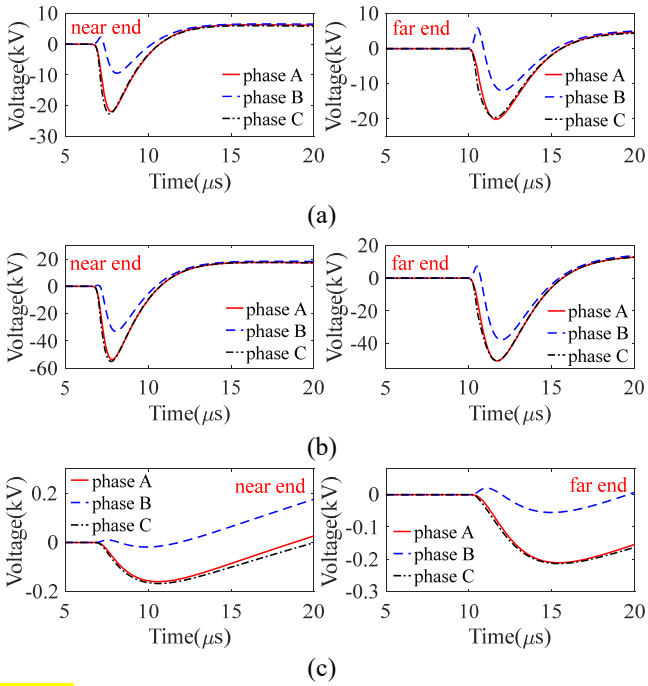

Fig. 11. When *p*=1, the coupling voltage at both ends on the overhead lines with different terminal loads excited by the SRS: (a) *R* loads; (b) *R-L* loads; (c) *R-C* loads.

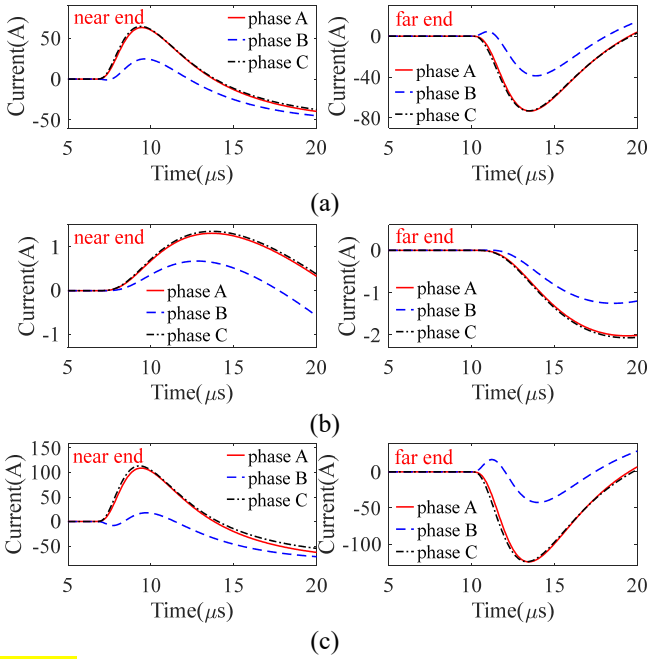

Fig. 12. When p=1, the coupling current at both ends on the overhead lines with different terminal loads excited by the FRS: (a) *R* loads; (b) *R-L* loads; (c) *R-C* loads.

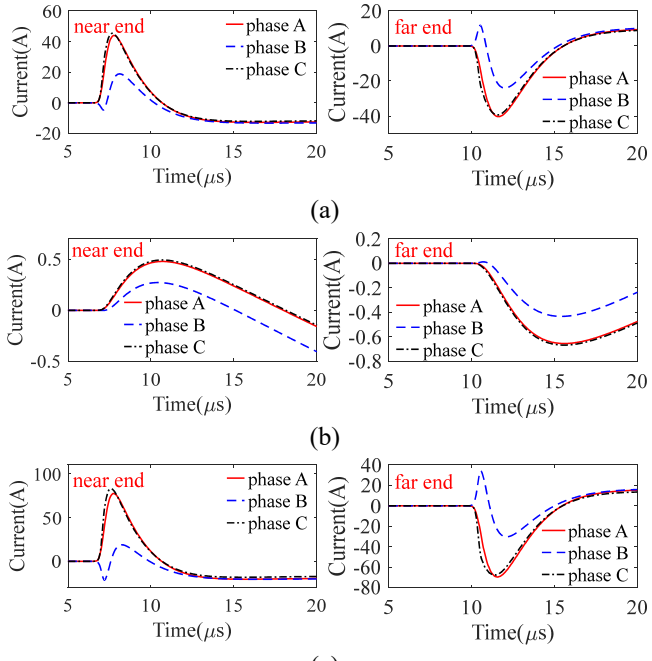

Fig. 13. When p=1, the coupling current at both ends on the overhead lines with different terminal loads excited by the SRS: (a) *R* loads; (b) *R-L* loads; (c) *R-C* loads.

Fig. 12 and Fig. 13 provide the coupling currents of each phase line excited by the FRS and the SRS. Apparently, the coupling current of *R-L* loads and *R-C* loads exhibit a completely opposite conclusion to the coupling voltage. Compared with overhead lines with *R* loads, the coupling currents of overhead lines with *R-L* loads significantly decrease, while the coupling currents of overhead lines with *R-C* load increase by nearly twice. The influence of *R-L* and *R-C* loads on coupling values of overhead lines at both ends can also provide a good reference for lightning protection.

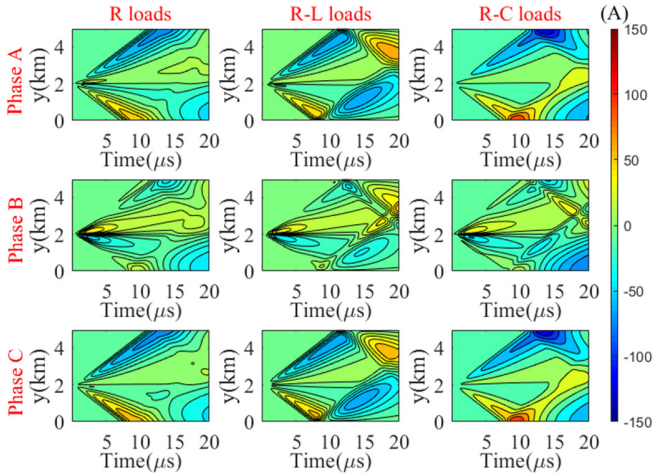

Fig. 14. When p=1, the coupling distribution current on the overhead lines with different terminal loads excited by the FRS.

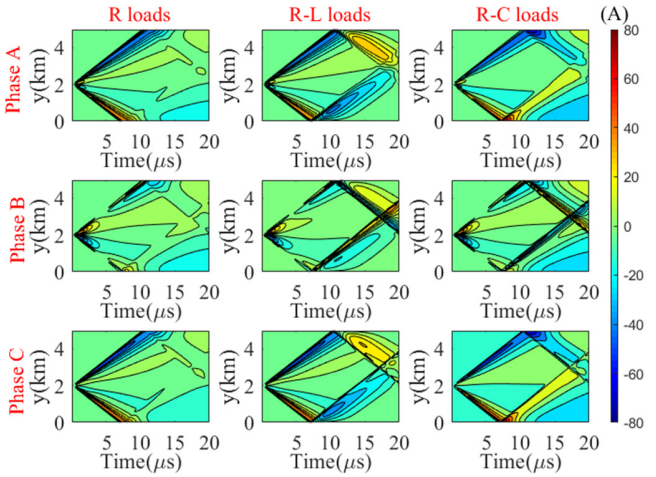

Fig. 15. When p=1, the coupling distribution current on the overhead lines with different terminal loads excited by the SRS.

The distribution of the coupling currents on overhead lines over time under three different loads is shown in Fig. 14 and Fig. 15. The difference in color represents the difference in current value. The coupling currents at the terminal start when the electromagnetic energy arrives. At the same time, the influence of the terminal loads on the coupling currents of the lightning EMF also starts from the arrival time of the lightning electromagnetic energy, and the loads will affect the coupling currents of the entire overhead lines.

It is worth noting that under the same load conditions, the current and voltage in phase B exhibit marked differences compared to those in phase A and phase C, as shown in Fig.10-Fig.15. This also indicates that in the scale variations of the studied model, the change in the height of overhead lines has a greater impact on the coupling value than the change in distance in the ρ-direction. Comparing the results, the amplitude of the coupling voltage excited by the FRS is larger, while the slope

of the curve excited by the SRS is larger and the change is more drastic. Therefore, the protection of the power system should simultaneously consider the impact of two types of return strokes.

C. The effect of different soil water percentage on the coupling voltage of overhead lines

After a large number of tests, six special soil water percentages with p=0.2, 1, 2, 5, 10, and 30 are selected for analysis because they can clearly and concisely show the influence of soil water percentage on the coupling value. Taking the more common *R-L* loads in the power system as an example, the influence of soil water percentage change on the response of the overhead lines terminal is analyzed, as shown in Fig.16 and Fig. 17. From the changing trend of the curve, it can be clearly seen that with the increase of soil water percentage, the terminal coupling voltage shows a change law that the value becomes larger and the absolute value first decreases and then increases. When the soil is in the range of low water percentage, such as 0.2%-1%, the coupling values of the overhead line are very sensitive to the change of soil water percentage, and when the soil is in the range of high water percentage, such as 5%-30%, the sensitivity of the coupling values of overhead lines is significantly reduced. Moreover, the curves in Fig.16 and Fig.17 consistently shift from a negative peak at low water percentages to a positive peak at high water percentages, which is mainly caused by the horizontal electric field.

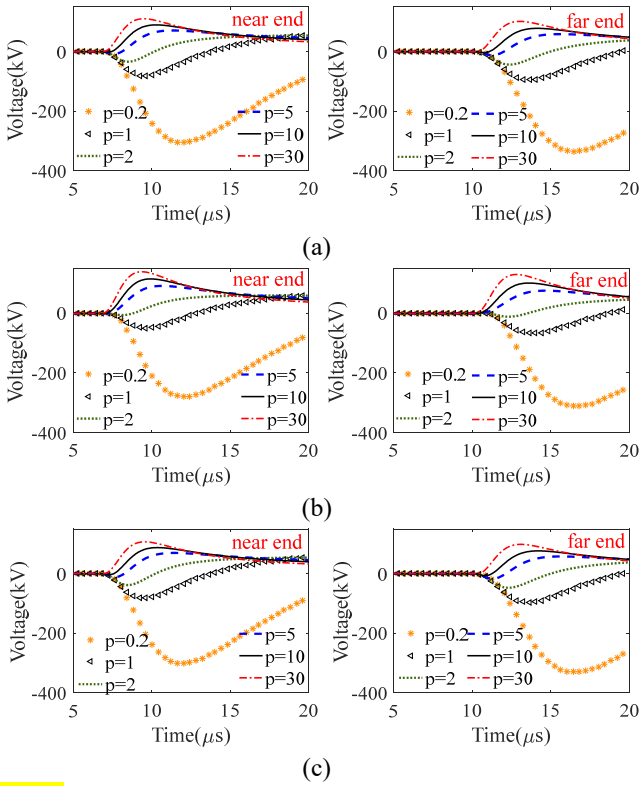

Fig. 16. The coupling voltage of both ends on the overhead lines with *R-L* loads excited by the FRS under different soil water percentages: (a) phase A; (b) phase B; (c) phase C.

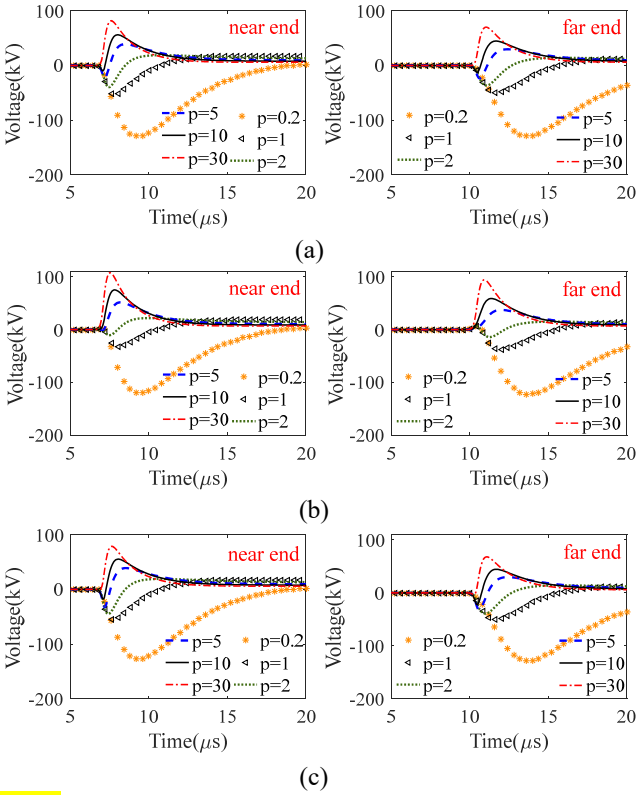

Fig. 17. The coupling voltage of both ends on the overhead lines with *R-L* loads excited by the SRS under different soil water percentages: (a) phase A; (b) phase B; (c) phase C.

V. CONCLUSION

This paper uses recursive convolution and FDTD technology to solve the coupling values of overhead lines above the dispersive ground excited by the FRS and the SRS considering the change of soil water percentage. Different from the conventional method for dealing with the convolution part of the governing equations of transmission lines, we combine the characteristics of the integration by parts method and the IW difference format to ensure that the iterative equation does not contain fraction related to the poles and residues after using the VF method. Our results are successfully validated by literature results. Taking a 35kV overhead lines model as an example, the influence of different terminal impedance types and soil water percentages on the coupling value is analyzed.

The results demonstrate that the coupling values of the overhead lines are more sensitive to the change of height than the change of horizontal distance. The coupling values of the overhead lines excited by the FRS are larger than that of the SRS, and the change of the coupling values of the SRS is more drastic. The *R-L* loads increase the coupling voltage of the overhead lines and reduce the coupling current compared to purely resistive loads, while *R-C* loads have the exact opposite effect. With the increase of soil water percentage, the coupling voltage values of the overhead lines become larger and larger, while the absolute values present a trend of decreasing first and then increasing. Furthermore, the coupling values of overhead lines are more sensitive to changes in water percentages at low water percentages than at high.

VI. APPENDIX

In the 2D cylindrical coordinate system, the differential format of electromagnetic waves generated by lightning is shown in Fig. 18. The difference format used for solving spatial EMFs is the leapfrog format, so it is necessary to Δt and the minimum value of Δz and $\Delta\rho$ should satisfy the Courant condition.

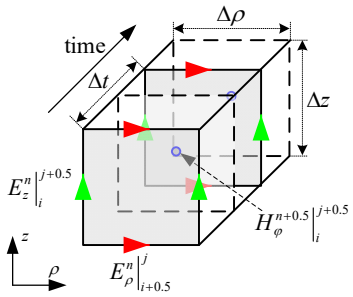

Fig. 18. Space and time difference relationship of lightning electromagnetic field.

A. Area to be solved

The magnetic field iterative equations for the air and soil parts are the same and can be written as:

$$H_\varphi^{n+0.5}\big|_{i+0.5}^{j+0.5}=H_\varphi^{n-0.5}\big|_{i+0.5}^{j+0.5}+\frac{\Delta t}{\mu_0\Delta\rho}\left(E_z^n\big|_{i+1}^{j+0.5}-E_z^n\big|_i^{j+0.5}\right)-\frac{\Delta t}{\mu_0\Delta z}\left(E_\rho^n\big|_{i+0.5}^{j+1}-E_\rho^n\big|_{i+0.5}^{j}\right) \quad (A.1)$$

The electric field iterative equation of the air part is:

$$E_\rho^{n+1}\big|_{i+0.5}^{j}=CA\cdot E_\rho^n\big|_{i+0.5}^{j}-\frac{CB}{\Delta z}\cdot\left(H_\varphi^{n+0.5}\big|_{i+0.5}^{j+0.5}-H_\varphi^{n+0.5}\big|_{i+0.5}^{j-0.5}\right) \quad (A.2)$$

$$E_z^{n+1}\big|_i^{j+0.5}=CA\cdot E_z^n\big|_i^{j+0.5}+\frac{CB}{\Delta\rho}\cdot\left[\left(1+\frac{1}{2i}\right)H_\varphi^{n+0.5}\big|_{i+0.5}^{j+0.5}-\left(1-\frac{1}{2i}\right)H_\varphi^{n+0.5}\big|_{i-0.5}^{j+0.5}\right] \quad (A.3)$$

The electric field iterative equation of the soil part is:

$$E_\rho^{n+1}\big|_{i+0.5}^{j}=CC\cdot\left[CD\cdot E_\rho^n\big|_{i+0.5}^{j}+\psi_\rho^n\big|_{i+0.5}^{j}-\frac{\Delta t}{\Delta z\varepsilon_0}\left(H_\varphi^{n+0.5}\big|_{i+0.5}^{j+0.5}-H_\varphi^{n+0.5}\big|_{i+0.5}^{j-0.5}\right)\right] \quad (A.4)$$

where

$$\psi_\rho^n\big|_{i+0.5}^{j}=E_\rho^n\big|_{i+0.5}^{j}\Delta\chi_0+\sum_{k=1}^{13}\exp(-2\pi f_k\Delta t)\psi_{\rho,k}^{n-1}\big|_{i+0.5}^{j} \quad (A.5)$$

$$\Delta\chi_0=\sum_{k=1}^{13}a_k\left(1-\exp(-2\pi f_k\Delta t)\right)^2 \quad (A.6)$$

$$E_z^{n+1}\big|_i^{j+0.5}=CC\cdot\left\{CD\cdot E_z^n\big|_i^{j+0.5}+\psi_z^n\big|_i^{j+0.5}+\frac{\Delta t}{\varepsilon_0\Delta\rho}\left[\left(1+\frac{1}{2i}\right)H_\varphi^{n+0.5}\big|_{i+0.5}^{j+0.5}-\left(1-\frac{1}{2i}\right)H_\varphi^{n+0.5}\big|_{i-0.5}^{j+0.5}\right]\right\} \quad (A.7)$$

$$\psi_z^n\big|_i^{j+0.5}=E_z^n\big|_i^{j+0.5}\Delta\chi_0+\sum_{k=1}^{13}\exp(-2\pi f_k\Delta t)\psi_{z,k}^{n-1}\big|_i^{j+0.5} \quad (A.8)$$

Left boundary of air part

$$E_z^{n+1}\big|_0^{j+0.5}=CA\cdot E_z^n\big|_0^{j+0.5}+4\frac{CB}{\Delta\rho}\cdot H_\varphi^{n+0.5}\big|_{0.5}^{j+0.5}-\frac{CE}{\Delta\rho}\cdot I_z\big|_0^{j+0.5} \quad (A.9)$$

Left boundary of soil part

$$E_z^{n+1}\big|_0^{j+0.5}=CC\cdot\left(CD\cdot E_z^n\big|_0^{j+0.5}+CE\cdot H_\varphi^{n+0.5}\big|_{0.5}^{j+0.5}+\psi_z^n\big|_i^{j+0.5}\right) \quad (A.10)$$

The coefficients are:

$$CA=(2\varepsilon-\sigma\Delta t)/(2\varepsilon+\sigma\Delta t) \quad (A.11)$$

$$CB=2\Delta t/(2\varepsilon+\sigma\Delta t) \quad (A.12)$$

$$CC=1/\left[\varepsilon_\infty+\chi_0+\Delta t\sigma_0/(2\varepsilon_0)\right] \quad (A.13)$$

$$CD=\varepsilon_\infty-\sigma_0\Delta t/(2\varepsilon_0) \quad (A.14)$$

$$CE=4\Delta t/(\varepsilon_0\Delta\rho) \quad (A.15)$$

B. CPML boundary

$$H_\varphi^{n+0.5}\big|_{i+0.5}^{j+0.5}=H_\varphi^{n-0.5}\big|_{i+0.5}^{j+0.5}+\frac{\Delta t}{\mu_0\Delta\rho\kappa_\rho}\left(E_z^n\big|_{i+1}^{j+0.5}-E_z^n\big|_i^{j+0.5}\right)-\frac{\Delta t}{\mu_0\Delta z\kappa_z}\left(E_\rho^n\big|_{i+0.5}^{j+1}-E_\rho^n\big|_{i+0.5}^{j}\right)-\frac{\Delta t}{\mu_0}\left(\psi_{H\varphi z}^n\big|_{i+0.5}^{j+0.5}-\psi_{H\varphi\rho}^n\big|_{i+0.5}^{j+0.5}\right) \quad (A.16)$$

where

$$\psi_{H\varphi z}^n\big|_{i+0.5}^{j+0.5}=b_z\psi_{H\varphi z}^{n-1}\big|_{i+0.5}^{j+0.5}+\frac{a_z}{\Delta z}\left(E_\rho^n\big|_{i+0.5}^{j+1}-E_\rho^n\big|_{i+0.5}^{j}\right) \quad (A.17)$$

$$\psi_{H\varphi\rho}^n\big|_{i+0.5}^{j+0.5}=b_\rho\psi_{H\varphi\rho}^{n-1}\big|_{i+0.5}^{j+0.5}+\frac{a_\rho}{\Delta\rho}\left(E_z^n\big|_{i+0.5}^{j+1}-E_z^n\big|_{i+0.5}^{j}\right) \quad (A.18)$$

$$E_\rho^{n+1}\big|_{i+0.5}^{j}=CA\cdot E_\rho^n\big|_{i+0.5}^{j}-CB\cdot\psi_{E\rho z}^{n+0.5}\big|_{i+0.5}^{j}-\frac{CB}{\Delta z\kappa_z}\cdot\left(H_\varphi^{n+0.5}\big|_{i+0.5}^{j+0.5}-H_\varphi^{n+0.5}\big|_{i+0.5}^{j-0.5}\right) \quad (A.19)$$

where

$$\psi_{E\rho z}^{n+0.5}\big|_{i+0.5}^{j}=b_z\psi_{E\rho z}^{n-0.5}\big|_{i+0.5}^{j}+\frac{a_z}{\Delta z}\left(H_\varphi^{n+0.5}\big|_{i+0.5}^{j+0.5}-H_\varphi^{n+0.5}\big|_{i+0.5}^{j-0.5}\right) \quad (A.20)$$

$$E_z^{n+1}\big|_i^{j+0.5}=CA\cdot E_z^n\big|_i^{j+0.5}+CB\cdot\left(\psi_{Ez\rho}^n\big|_i^{j+0.5}+\psi_{Ez\varphi}^n\big|_i^{j+0.5}\right)+CB\cdot\left(\frac{\kappa_\rho/i+2\kappa_\varphi}{2\kappa_\rho\kappa_\varphi\Delta\rho}H_\varphi^{n+0.5}\big|_{i+0.5}^{j+0.5}+\frac{\kappa_\rho/i-2\kappa_\varphi}{2\kappa_\rho\kappa_\varphi\Delta\rho}H_\varphi^{n+0.5}\big|_{i-0.5}^{j+0.5}\right) \quad (A.21)$$

where

$$\psi_{Ez\rho}^{n+0.5}\big|_i^{j+0.5}=b_\rho\psi_{Ez\rho}^{n-0.5}\big|_i^{j+0.5}+\frac{a_\rho}{\Delta\rho}\left(H_\varphi^{n+0.5}\big|_{i+0.5}^{j+0.5}-H_\varphi^{n+0.5}\big|_{i-0.5}^{j+0.5}\right) \quad (A.22)$$

$$\psi_{Ez\varphi}^{n+0.5}\big|_i^{j+0.5}=b_\varphi\psi_{Ez\varphi}^{n-0.5}\big|_i^{j+0.5}+\frac{a_\varphi}{2\rho_i}\left(H_\varphi^{n+0.5}\big|_{i+0.5}^{j+0.5}+H_\varphi^{n+0.5}\big|_{i-0.5}^{j+0.5}\right) \quad (A.23)$$

$$\kappa_u=1+\kappa_{\max}(u-u_0)^{n_p}/d^{n_p}\quad u=\rho,z \quad (A.24)$$

$$\kappa_\varphi=1+\kappa_{\max}(\rho-\rho_0)^{n_p}/\left[(n_p+1)\rho d^{n_p}\right] \quad (A.25)$$

$$\sigma_u=\sigma_{\max}(u-u_0)^{n_p}/d^{n_p}\quad u=\rho,z \quad (A.26)$$

$$\sigma_\varphi=\sigma_{\max}(\rho-\rho_0)^{n_p+1}/\left[(n_p+1)\rho d^{n_p}\right] \quad (A.27)$$

$$b_u=\exp\left[-(\sigma_u/\kappa_u+\alpha_u)\Delta t/\varepsilon_0\right]\quad u=\rho,\varphi,z \quad (A.28)$$

$$a_u=\sigma_u(b_u-1)/(\sigma_u\kappa_u+\kappa_u^2\alpha_u)\quad u=\rho,\varphi,z \quad (A.29)$$

where $\kappa_{\max}$ is a constant greater than 1, which can be obtained by trial and error method, and d is the thickness of the CPML. ρ_0 and z_0 denote the interface between FDTD and CPML. n_p is the order of polynomial. In the above equations, the electric parameter value of the solution area is determined by its constituent medium.

REFERENCES

[1] J. Wang, Y. Zhao, Y. Fang, L. Cai, S. Wang, Z. Xu and Si Cheng, "Observation of overvoltage at the terminal of 10 kV distribution line by direct triggered lightning," *IEEE Trans. Power Deliv.*, vol. 37, no. 5, pp. 3547-3554, Oct. 2022.

[2] M. Nazari, R. Moini, S. Fortin, F. P. Dawalibi, and F. Rachidi, "Impact of frequency-dependent soil models on grounding system performance for direct and indirect lightning strikes," *IEEE Trans. Electromagn. Compat.*, vol. 63, no. 1, pp. 134–144, Feb. 2021.

[3] F. Delfino, R. Procopio, M. Rossi, and F. Rachidi, "Influence of frequency-dependent soil electrical parameters on the evaluation of lightning electromagnetic fields in air and underground," *J. Geophys. Res. Atmospheres*, vol. 114, no. D11, 2009.

[4] T. F. Garbelim Pascoalato, A. R. Justo de Araújo, P. T. Caballero, J. S. Leon Colqui, and S. Kurokawa, "Transient analysis of multiphase transmission lines located above frequency-dependent soils," *Energies*, vol. 14, no. 17, p. 5252, Aug. 2021.

[5] Z. Sun, L. Shi, Y. Zhou, B.Yang, and W. Jiang, "FDTD evaluation of LEMP considering the lossy dispersive ground," *Appl. Comput. Electromagn. Soc. J. ACES*, pp. 7–14, 2018.

[6] Mohammad E. M. Rizk, Sayed Abulanwar, Abdelhady Ghanem, and Matti Lehtonen, "Computation of lightning-induced voltages considering ground impedance of multi-conductor line for lossy dispersive soil," *IEEE Trans. Power Deliv.*, vol. 37, no. 4, pp. 2464–2473, Aug. 2022.

[7] J. P. L. Salvador, R. Alipio, A. C. S. Lima, and M. T. Correia de Barros, "A concise approach of soil models for time-domain analysis," *IEEE Trans. Electromagn. Compat.*, vol. 62, no. 5, pp. 1772–1779, Oct. 2020.

[8] M. Akbari, K. Sheshyekani, A. Pirayesh, F. Rachidi, M. Paolone, A. Borghetti, and C. A. Nucci, "Evaluation of lightning electromagnetic fields and their induced voltages on overhead lines considering the frequency dependence of soil electrical parameters," *IEEE Trans. Electromagn. Compat.*, vol. 55, no. 6, pp. 1210–1219, Dec. 2013.

[9] C. L. Longmire and K. S. Smith, "A universal impedance for soils:," defense technical information center, Fort Belvoir, VA, Oct. 1975.

[10] B. Yang, B. Zhou, C. Gao, L. Shi, B. Chen, and H. Chen, "Using a Two-Step Finite-Difference Time-Domain Method to Analyze Lightning-Induced Voltages on Transmission Lines," *IEEE Trans. Electromagn. Compat.*, vol. 53, no. 1, pp. 256–260, Feb. 2011.

[11] A. Sommerfeld, *Partial differential equations in physics*. New York: Academic press, 1949.

[12] M. N. O. Sadiku, A simple introduction to finite element analysis of electromagnetic problems, *IEEE Trans. Educ.*, Vol. 32, No. 2, pp. 85-93, 1989.

[13] K. Sheshyekani and M. Akbari, "Evaluation of lightning-induced voltages on multiconductor overhead lines located above a lossy dispersive ground," *IEEE Trans. Power Deliv.*, vol. 29, no. 2, pp. 683–690, Apr. 2014.

[14] K. S. Yee, Numerical solution of initial boundary value problems involving Maxwell's equations in isotropic media, *IEEE Trans. Antennas Propag.*, Vol. AP-14, No. 3, pp 302-307, May, 1966.

[15] C. Yang and B. Zhou, "Calculation methods of electromagnetic fields very close to lightning," *IEEE Trans. Electromagn. Compat.*, vol. 46, no. 1, pp. 133–141, Feb. 2004.

[16] J. Liu, G. Wan, J. Zhang, and X. Xi, "An Effective CFS-PML implementation for cylindrical coordinate FDTD method," *IEEE Microw. Wirel. Compon. Lett.*, vol. 22, no. 6, pp. 300–302, Jun. 2012.

[17] L. Huang, C. Gao, J. Wang, F. Guo, and Q. Zhang, "Simulation of LEMP by using FDTD method with CPML in the 2-D cylindrical coordinate system," in *2018 IEEE International Conference on Computational Electromagnetics (ICCEM)*, Mar. 2018, pp. 1–3.

[18] L. Huang, J. Wang, F. Guo, Q. Zhang, and C. Gao, "A new inversion algorithm for estimating the return-stroke velocity," *IEEE Trans. Electromagn. Compat.*, vol. 61, no. 5, pp. 1524–1533, Oct. 2019.

[19] J. A. Roden and S. D. Gedney, "Convolution PML (CPML): An efficient FDTD implementation of the CFS–PML for arbitrary media," *Microw. Opt. Technol. Lett.*, vol. 27, no. 5, pp. 334–339, 2000.

[20] O. Kurnaz and S. Aksoy, "Debye Representation of Frequency Dependent Ground for LEMP Analysis With RC-FDTD," *IEEE Trans. Electromagn. Compat.*, vol. 64, no. 6, pp. 2149–2156, Dec. 2022.

[21] R. Alipio, A. D. Conti, and F. Rachidi, "Simulation of High-Frequency Transients in Overhead Lines Including Frequency-Dependent Soil Parameters: a FDTD Approach," in *2021 35th International Conference on Lightning Protection (ICLP) and XVI International Symposium on Lightning Protection (SIPDA)*, Sep. 2021, pp. 01–06.

[22] C. R. Paul, *Analysis of multiconductor transmission lines*, 2. ed. in Wiley-Interscience. Hoboken, NJ: Wiley, 2008.

[23] D. Deschrijver, M. Mrozowski, T. Dhaene, and D. De Zutter, "Macromodeling of multiport systems using a fast implementation of the vector fitting method," *IEEE Microw. Wirel. Compon. Lett.*, vol. 18, no. 6, pp. 383–385, Jun. 2008.

[24] C. Yang, F. Zhu, N. Lu and Y. Yang, "Analysis on uncertainty of field-to-wire coupling model in time domain," *IEEE Trans. Power Deliv.*, vol. 37, no. 5, pp. 3771–3781, Oct. 2022.

[25] F. Rachidi, C.A. Nucci, M. Ianoz, and C. Mazzetti, "Influence of a lossy ground on lightning-induced voltages on overhead lines," *IEEE Trans. Electromagn. Compat.*, vol. 38, no. 3, pp. 250–264, Aug. 1996.

[26] A. Agrawal, H. Price, and S. Gurbaxani, "Transient Response of Multiconductor Transmission Lines Excited by a Nonuniform Electromagnetic Field," *IEEE Trans. Electromagn. Compat.*, vol. EMC-22, no. 2, pp. 119–129, May 1980.

[27] X. Liu, M. Zhang, T. Wang, and Y. Ge, "Fast evaluation of lightning-induced voltages of overhead line and buried cable considering the lossy ground," *IET Sci. Meas. Technol.*, vol. 13, no. 1, pp. 67–73, Jan. 2019.

[28] F. Tossani, F. Napolitano, and A. Borghetti, "Inverse Laplace Transform of the Ground Impedance Matrix of Overhead Lines," *IEEE Trans. Electromagn. Compat.*, vol. 60, no. 6, pp. 2033–2036, Dec. 2018.

[29] M. Paolone, F. Rachidi, A. Borghetti, C. A. Nucci, M. Rubinstein, V. A. Rakov and M. A. Uman, "Lightning Electromagnetic Field Coupling to Overhead Lines: Theory, Numerical Simulations, and Experimental Validation," *IEEE Trans. Electromagn. Compat.,* vol. 51, no. 3, pp. 532-547, Aug. 2009.

[30] G. Yang, Z. Yu, Y. Zhang, S. Chen, B. Zhang, and J. He, "Evaluation of lightning current and return stroke velocity using measured far electric field above a horizontally stratified ground," *IEEE Trans. Electromagn. Compat.*, vol. 59, no. 6, pp. 1940–1948, Dec. 2017.